Reduction of Manganese Ores in CO-CO_2 Atmospheres

TRINE ASKLUND LARSSEN, DIETER SENK, and MERETE TANGSTAD

The reduction of higher manganese oxides to MnO in the prereduction zone of a ferromanganese furnace is largely decisive for the overall energy efficiency and climate gas emissions for the overall production process. Kinetics of the gas-solid reaction between the ore and CO(g) in the ascending furnace gas is dependent on the ore characteristics. The aim of this study was to elucidate the reduction steps during prereduction of two commercial manganese ores, Comilog and Nchwaning, in CO-CO_2 atmosphere. Ore samples in various size fractions were exposed to isothermal and non-isothermal temperature regimes in various gas atmospheres utilizing a thermogravimetric furnace. Samples were characterized by titration, XRF, XRD, and SEM analyses. Comilog is a high oxygen ore, where the majority of the ore is constituted by various tetravalent manganese minerals. When heated in reducing atmosphere, MnO_2-oxides were reduced to MnO in a single step at temperatures below 550 °C. The rate was dependent on the particle size and CO-concentration. When the temperature reached 550 °C, any present MnO_2 rapidly decomposed to Mn_2O_3, which further continued to reduce to MnO. Nchwaning ore was found to be mainly constituted by Mn_2O_3-oxides, calcite and hematite. Manganese- and iron-oxides were found to reduce at similar temperature ranges, however the manganese oxide reduction was initiated prior to the iron oxides in smaller particle sizes (< 4 mm). Trivalent manganese oxides reduced to MnO in a single step, and the reduction of iron oxides subsided with the formation of wüstite. Carbonates decomposed at temperature range 800 °C to 1000 °C. Both ores obtained a promoted reaction rate with decreasing particle size and increased pctCO in CO-CO_2 atmosphere.

https://doi.org/10.1007/s11663-020-02018-0

I. BACKGROUND

MANGANESE ferroalloys are produced in submerged arc furnaces, where the carbon and energy consumption of the process will be largely dependent on the solid-state reduction of manganese ore at relatively low temperatures. Higher manganese oxides (MnOx, $x > 1$) in the ore will reduce to MnO by CO(g) present in the furnace gas when exposed to elevated temperatures. The reduction's influence on the efficiency is two-fold. Firstly, the reduction reactions are exothermic, thus heating the charge material and minimizing the required electric energy feed. This implies that the heat production is dependent on the oxygen level of the ore. Secondly, CO_2(g) produced from the reduction reactions may be consumed by the Boudouard reaction (CO_2(g) + C = 2CO(g)), which is both carbon consuming and highly endothermic. It is generally agreed that the Boudouard reaction obtains sufficient kinetics at temperatures exceeding 800 °C in a ferromanganese furnace.[1,2] Kinetics and mechanisms of the ore-gas reduction is dependent on the properties of the ore.

Geology and geochemistry of different commercial manganese ores and minerals have been presented in a number of previous publications. Certain studies reporting on mineralogy of manganese ores provide the main constituting minerals,[3–5] whereas others provide quantitative measures of both major and minor phases.[6,7] In general, these studies have shown that characterization of manganese ores is not a straight-forward procedure. A great number of minerals is found to constitute the same ore, where both highly similar composition of several minerals, cation substitution, heterogeneity of the ore, as well as geometric effects, such as porosity and cracks, complicates the characterization process. Varentsov and Grasselly[8] presented a review of existing literature on characteristics of the most common manganese minerals, where it was stated that several of the minerals are frequently intergrown. Waldemar and Dressel[9] investigated the thermal behavior of various

TRINE ASKLUND LARSSEN and MERETE TANGSTAD are with the Norwegian University of Science and Technology (NTNU), 7034 Trondheim, Norway. DIETER SENK is with the RWTH Aachen University, 52062 Aachen, Germany Contact e-mail: trine.a.larssen@sintef.no

Manuscript submitted May 28, 2020; accepted October 18, 2020.
Article published online November 20, 2020.

manganese minerals in controlled atmospheres, reporting that the reduction/decomposition behavior of the minerals was affected by the presence of other minerals. Mineralogy of Nchwaning and Gloria manganese ores obtained through XRD were reported by Visser *et al.*,[6] who identified ten different constituting minerals, of which five were considered of minor abundance (< 5 pct). Nchwaning ore was mainly composed of braunite and braunite II, whereas Gloria contained braunite, as well as considerable amounts of calcite and kutnahorite. A low correlation between XRD and SEM/EDS analyses was presented by Sørensen *et al.*[7] According to XRD, Groote Eylandt ore was found to be fully composed by pyrolusite, however, optical and SEM analysis showed that the ore contained pyrolusite, cryptomelane, iron alumo-silicates, and quartz. It was further observed that XRD identified bixbyite as main mineral of Wessels ore, whereas SEM and EDS investigations showed that the mineral identified as bixbyite was in fact braunite in two different modifications.

The reduction behavior of manganese ores is complex due to multistep and parallel reaction schemes. High oxygen ores, such as Comilog, contains large abundance of tetravalent oxides (MnO_2), and may reduce through oxidation sequence MnO_2-Mn_2O_3-Mn_3O_4-MnO, whereas semi-oxidized ores, such as Nchwaning, generally contains trivalent oxides (Mn_2O_3), thus omitting the first reduction step. On the other hand, these semi-oxidized ores often contains significant amount of iron oxides, which may reduce through sequence Fe_2O_3-Fe_3O_4-FeO-Fe. Several experimental studies have been reported regarding prereduction of manganese ores in CO-CO_2 atmosphere, both in isothermal[2,5,10,11] and non-isothermal[6,12–16] temperature regimes. Non-isothermal studies have commonly been used to simulate the industrial furnace conditions, *i.e.* to evaluate whether the ores will continue to reduce in the active region of the Boudouard reaction, often defined as the CO-reactivity of the ore. These studies generally provide little or no information of kinetics and mechanisms. They do however provide an overview of the reduction extent obtained at a given temperature, commonly 800 °C, for various commercial manganese ores. The studies show that Comilog ore has a higher CO-reactivity compared to Nchwaning ore. According to Turkova, Slizovskiy, and Tangstad this may be explained by the higher porosity of Comilog ore compared to Nchwaning ore, as the authors reported a lower oxygen level at 800 °C, *i.e.* higher reduction degree, with increasing initial porosity of the ores.[13] Isothermal conditions are commonly used to simplify the mathematical interpretation of reaction mechanisms and kinetics by avoiding temperature as a variable. As such, all studies reporting on kinetics and mechanisms of manganese ores have been conducted in isothermal temperature regimes. Several studies have been performed where the ore has been calcined prior to the reduction experiments, as the aim was to investigate the reduction of Mn_3O_4 to MnO, which is the reduction step that may occur simultaneously as the Boudouard reaction. Thus, less information is available on the initial reduction steps, such as MnO_2 and Mn_2O_3. In addition, studies have shown that reduction behavior is dependent on the pretreatment of the ore, implying that relevant and representative data may not be obtained from calcined or synthetic materials.[2,12,17] Another aspect shared by the studies is the fairly high temperatures at which the experiments have been conducted, implying that the extent of information regarding the ores behavior as it is being fed to the furnace is low.

The literature review shows that the reduction of manganese ores have been investigated in both no-isothermal and isothermal experiments. Non-isothermal studies provide information on the extent at which the ore reduces at temperatures exceeding 800 °C, but provides no or little information on the reaction mechanisms. Isothermal studies have generally been conducted using pretreated (or synthetic) manganese materials, which have been observed to exhibit dissimilar reduction behavior compared to the untreated ores. Further, these studies have been conducted at fairly high temperatures, close to the melting point of the ores. As such, information on the behavior of the ore as it is fed to the industrial furnace is scarce.

This study aims to determine the reduction path of reduction of Comilog and Nchwaning manganese ores in CO-CO_2 atmosphere. The focus is on phase compositions of ores and changes observed when the ore is exposed to elevated temperatures and CO(g).

II. EXPERIMENTAL

Comilog- and Nchwaning-ore were investigated in CO-CO_2 atmosphere under isothermal and non-isothermal temperature regimes. The majority of the experimental work was carried out at NTNU, whereas parts of the work (isothermal reduction experiments) were conducted at RWTH Aachen. All characterization of reduced samples were performed at NTNU.

The ores were ground and sieved into three different particle size fractions, *i.e.* 0.50 to 1.36, 3.33 to 4.00, and 11.20 to 15.00 mm. Chemical composition was determined by X-ray Fluorescence, except for MnO_2, CO_2, H_2O and LOI content. MnO_2 was determined by titration (ASTM 465-11:2017), whereas H_2O and LOI were determined by thermogravimetry. Eltra (combustion-IR) was used to determine amount of carbon, which was recalculated to CO_2. The content of light elements, such as lithium and hydrogen, is not quantified by XRF due to low energy levels. As such, the amount of chemically bound moisture in the ores was estimated by heating approximately 10 g of sample in air in a muffle furnace at 950 °C for 12 hours. It was assumed that the registered weight loss included removal of volatiles (surface and bound moisture, and CO_2), as well a contribution from manganese and iron oxide reduction. The extent of weight loss attributed to manganese and iron oxides was determined by titration. Hence, the content of chemically bound moisture may be calculated, as all remaining components of the total weight loss is accounted for.

Mineralogy was determined by X-ray diffraction (XRD), where the specific instrument was a Bruker D8 A25 DaVinci X-ray Diffractometer with CuKα-radiation. The instrument has a LynxEye™ SuperSpeed Detector. Mineral identification was performed using the PDF database in the BRUKER EVA program. Quantitative results were obtained using Rietveld analysis in Topas 5 software. For some of the identified phases, no information on the crystal structure was available in the utilized database. In these cases, values were retrieved from the AMS Crystal Stucture Database. This enables data for all identified phases, except for nsutite, a mineral present in untreated Comilog ore, which does not have a defined crystal structure. Samples were prepared for scanning electron microscope by mounting in epoxy resin mold, which were subjected to a vacuum chamber before hardening. The samples were ground and polished, washed with water and soap, and lastly rinsed with ethanol. Hardened samples were coated with carbon and investigated by SEM/EDS. The specific instrument was a FE-SEM (Zeiss Ultra 55 LE) with a Bruker EDS/NORDIF EBSD system. An acceleration voltage of 15 kV was applied. It is known that light elements ($Z < 11$), such as oxygen and hydrogen, are not accurately quantified by EDS. Further, representative carbon contents are not obtained when the sample has been carbon coated. Another aspect of quantitative analysis of manganese ores is the geometric effects encountered due to concentration of porosity and cracks, which will lead to unreliable data. According to Newbury and Ritchie,[18,19] a strong indicator of the severity of geometric effects is the raw analytical total that is obtained. They observed that the deviation of the obtained normalized concentration was strongly correlated to the analytical total, where the relative errors fell within 20 pct or less of the correct value provided that the raw analytical total was within range 80 to 120 pct. As such, less attention is paid to the specific quantified concentration of different elements by EDS in this study. Rather, the focus has been the relation between different elements identified in the same analysis.

Non-isothermal reduction experiments were conducted in a vertical retort tube furnace, connected to a thermobalance and off-gas analyzer. The sample (75 g) was located in the lower parts of the crucible, placed on top of a grid in order to ensure an even distribution of the gas. The gas inlet is at the top of the crucible, from where the gas moves through the double walls, meeting the sample from the bottom. The exiting gas leaves through a gas-analyzer (NDIR), continuously measuring the CO-CO_2 concentrations in the gas. A schematic and description of the furnace may be found elsewhere.[13] A heating rate of 6 °C/min was applied for all experimental runs. The majority of the experiments were terminated at 1000 °C, however certain repeated experiments were terminated at a lower temperature in order to examine developing phases and structure. Samples were exposed to a gas flow of 4 Nl/min containing 50 or 80 pct CO, with remainder being CO_2. When target temperature was reached, the power supply was disconnected and the gas was replaced by a 4 Nl/min flow of argon during cooling. It was observed that the thermobalance was subjected to drifting, which was inconsistent both in terms of extent and duration. As such, it was decided to rely on the off-gas analysis, as the extent of prereduction of manganese ores is reflected by the CO/CO_2 ratio. The weight behavior obtained from the off-gas was normalized to the weight loss found from weighing of sample prior and subsequent to the reduction experiments.

Isothermal reduction experiments were conducted in the Tammann furnace facility at IEHK RWTH Aachen. The furnace is a thermogravimetric open tube furnace. Comilog and Nchwaning ore in size fraction 11.20 to 15.00 mm were reduced in CO-CO_2 atmosphere, where CO-concentration were 50 or 70 pct. A tungsten or Kanthal mesh wire was used to construct a sample holder from which the sample was suspended from an electronic mass balance during the experiments. The gas mixture was adjusted by mass flow controllers before entering the furnace chamber from the lower parts. A thermocouple was located in the chamber at the same height as the sample. A schematic of the furnace is found elsewhere.[20] 4 to 5 ore particles were evaluated in each experimental run at temperatures 400 °C to 900 °C. The smaller sample size was used mainly due to limitations of furnace geometry. It is further believed that a smaller sample size provides a more stable temperature, as less heat is evolved. Following 20 to 60 minutes holding time, the samples were removed from the chamber and cooled in a separate container while flushed in argon. Due to small sample size and furnace geometry, the weight reduction data was subjected to a high degree of fluctuations. As such, the results from isothermal reduction are discussed in terms of the composition and mineralogy of the reduction products.

III. RESULTS AND DISCUSSION

A. *Comilog Ore*

1. *Characterization of ore*

Comilog is a high-level oxygen ore with a manganese content of approximately 50 pct, where the oxygen level (x in MnO_x) is 1.94 to 1.95 (Table I). CaO and MgO are present in negligible amounts, whereas SiO_2 and Al_2O_3 are detected in concentrations between 3.5 to 6.6 pct. The content of chemically bound H_2O was estimated to 5.0 pct. Phases identified by XRD were cryptomelane(KMn_8O_{16}), pyrolusite(MnO_2), ramsdellite(MnO_2), nsutite($Mn^{4+}_{1-x}Mn^{2+}_{x}O_{2-2x}(OH)_{2x}$), gibbsite($Al(OH)_3$), goethite($Fe(OH)_2$), quartz($SiO_2$), and lithiophorite($(Al,Li)MnO_2(OH)_2$). As may be seen in Figure 1, the XRD spectrum of Comilog ore results in wide diffraction peaks, thus complicating the identification process, particularly for phases of minor abundance. The broad peaks may arise from varying cation substitution, small crystallite sizes, peak overlaps, and/or content of amorphous phase.

There is a number of different X-ray diagrams for nsutite, $(Mn^{4+}_{1-x},Mn^{2+}_{x})O_{2-x}(OH)_{2x}$, as the crystal structure is composed of statistically distributed layers of tetragonal pyrolusite and orthorhombic ramsdellite. This gives rise to variance in crystallite size, layering

Table I. Chemical Composition of Comilog and Nchwaning Ore

		Comilog			Nchwaning		
		0.50 to 1.36 mm	3.33 to 4.00 mm	11.20 to 15.00 mm	0.50 to 1.36 mm	3.33 to 4.00 mm	11.20 to 15.00 mm
Mn	TOT	48.4	51.4	51.0	46.7	46.5	46.4
Fe	TOT	3.5	2.8	3.1	9.6	9.5	10.0
LOI (950 °C)	pct	12.8	12.5	13.0	4.1	4.0	4.0
MnO_2	pct	71.7	76.6	76.4	35.5	34.2	34.6
MnO	pct	3.9	3.8	3.5	31.3	32.2	31.6
Fe_2O_3	pct	5.0	4.0	4.4	13.7	13.6	13.4
SiO_2	pct	5.6	3.5	3.5	6.4	6.2	6.7
Al_2O_3	pct	6.6	5.6	5.6	0.5	0.5	0.5
CaO	pct	0.1	0.1	0.1	6.2	6.3	5.9
MgO	pct	0.2	0.2	0.1	1.1	1.1	1.0
P	pct	0.1	0.1	0.1	0.0	0.0	0.0
S	pct	0.0	0.0	0.0	0.1	0.2	0.1
TiO_2	pct	0.2	0.1	0.1	0.0	0.0	0.0
K_2O	pct	1.1	1.1	0.7	0.0	0.0	0.0
BaO	pct	0.2	0.2	0.3	0.5	0.5	0.4
CO_2	pct	0.2	0.2	0.1	3.2	3.2	3.0
H_2O(Free)	pct	0.4	0.6	0.2	0.0	0.0	<0.1
H_2O (Bound)	pct	5.0	5.0	5.0	0.0	0.0	0.0
Total	pct	100.2	101.2	100.2	98.2	97.0	97.3

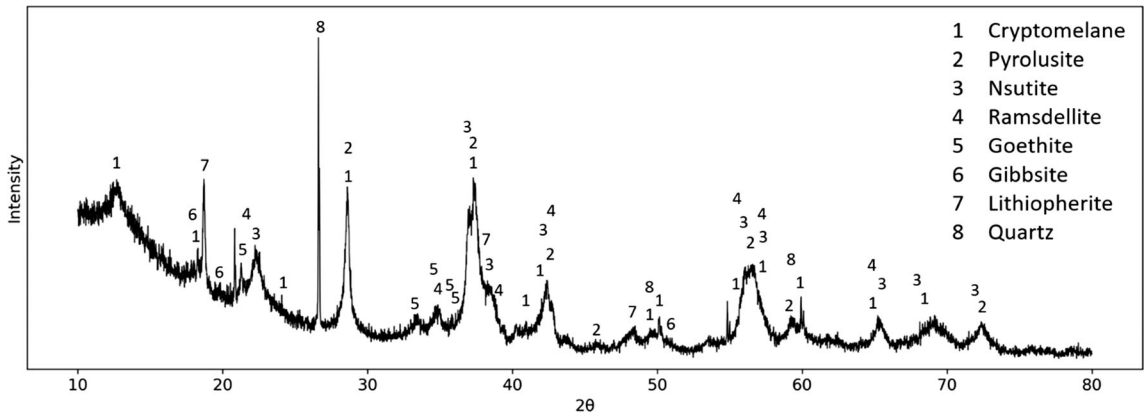

Fig. 1—XRD spectrum of Comilog ore (size 11.20 to 15.00 mm) with identified phases.

structure, and deviation from stoichiometric composition, which affects position, profile and intensity in XRD reflexes.[8] An estimation of the nsusite content is possible through what is known as peak-shape fitting, however as this causes the results to be highly unreliable, and requires considerable efforts, it was not performed in the present study. From visual observation of the peak intensities, cryptomelane, nsutite, and pyrolusite were determined to be the main Mn-bearing minerals. Smaller amounts of ramsdellite and lithiophorite were detected. Silicon is found in quartz, whereas iron is detected as goethite. The obtained mineralogy is in high accordance with the mineralogy reported by Sørensen *et al.*[7].

Cross-section examinations were performed on particles of size fraction 0.50 to 1.36 mm mounted in epoxy under a light microscope in order to get an overview of the various structures observed in Comilog ore. A large variance of microstructures were observed, as can be seen in Figure 2. Similar structures were observed in particle size 3.33 to 4.00 mm and 11.20 to 15.00 mm, however with a higher degree of heterogeneity. Figure 3 shows the cross-section of an 11.20 to 15.00 mm particle as observed through back scatter imaging. A complex and disorganized microstructure with high porosity is seen. Several of the minerals reported by XRD have highly similar compositions, which inhibits differentiation through EDS. In addition, cryptomelane,

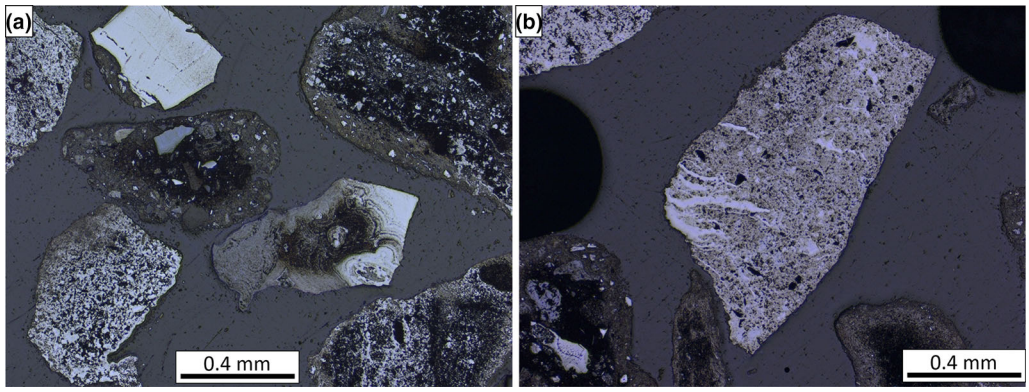

Fig. 2—A and B shows microstructure of Comilog ore particles (0.50 to 1.36 mm) as observed in light microscope. Scalebar reads 0.4 mm.

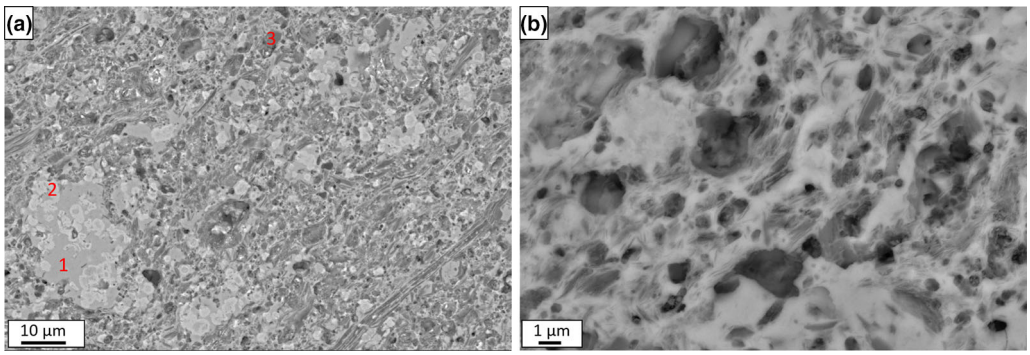

Fig. 3—Microstructure of Comilog ore (11.20 to 15.00 mm) obtained by backscatter imaging in scale of (*a*) 10 μm and (*b*) 1 μm.

pyrolusite, nsutite, and lithiophorite are reported to be frequently intergrown,[8] which may contribute to the lack of clear phase boundaries. The small grain diameter indicates that the EDS point analyses may be influenced by underlying phases. Selected analyses are presented in Table II, where it is seen that the phase identified as cryptomelane contains 4.5 at. pct Al. The brighter grey regions(area 2) within the cryptomelane were found to contain mainly iron and oxygen. As EDS does not provide reliable measures of oxygen and hydrogen, this phase was suggested to be goethite as this was the only iron phase identified by XRD. Due to few clear phase boundaries, element mapping was performed on the same particle, which showed that aluminium is present throughout the structure, except for areas rich in iron (Figure 4). Areas rich in iron correlate to low concentrations of other cations, indicating that iron is found as goethite, in accordance with XRD. Silicon is observed in co-existence with potassium and aluminium. Silicon is mainly found as quartz in Comilog ore, however due to the heterogeneous nature of the ore, quartz is not present in all particles.

2. *Weight reduction behavior*

Non-isothermal weight reduction behavior of Comilog ore at temperatures up to 1000 °C is presented in Figure 5. The correlating reaction rate, presented in Figure 6, was calculated as a change in weight at a 2-minute interval, where it was observed that all characteristics present at smaller time frames remained present. From the curves, it is evident the reduction of Comilog ore is promoted by decreasing particle size. All three particle sizes obtain a stable weight at temperatures exceeding 800 °C, indicating a complete prereduction to MnO. The weight reduction curves indicate a low, but significant, dependency on the CO partial pressure, as seen in the weight loss as a function of time. A higher reduction rate is obtained when reduced in 80 pct CO compared to 50 pct CO (Figure 6), however the temperature range at which reduction is ongoing is independent of CO-concentration. This may be due to the fact that the temperature is dependent on the reduction rate due to exothermic reactions, especially for Comilog ore. The reduction rate is considerably lower for particle size 11.20 to 15.00 mm, where a maximum of 0.7 wt pct/min is obtained compared to 3.8 wt pct/min for particle size 0.50 to 1.36 mm reduced in 80 pct CO. The curves for particle size 11.20 to 15.00 mm indicate that the reduction occurs through two distinct steps, where the first is initiated at 200 °C. A steep increase in the reaction rate is observed between 550 °C and 600 °C, indicating a second reduction step. The first stage may potentially be composed of two individual reactions, as the curve indicates the presence of two individual peaks at 310 °C and 410 °C, respectively. If all tetravalent oxides in Comilog ore show

Table II. Chemical Composition of Phases in Comilog Ore (11.20 to 15.00 mm) According to EDS Point Analysis (Average of 3 to 5 Point Analyses)

	Values from EDS								Proposed phase	
	Mn [At. Pct]	Fe [At. Pct]	Si [At. Pct]	Al [At. Pct]	O [At. Pct]	K [At. Pct]	Stoichiometry from EDS	Total [Wt Pct]	Mineral	Stochiometry
1	34.9	0.0	2.0	4.5	56.2	2.1	$KAl_2Mn_{16}O_{26}$	83.6	Cryptomelane	KMn_8O_{16}
2	6.9	38.6	0.5	1.4	51.9	0.2	$(Fe,Mn)_{0.9}O$	90.9	goethite	$Fe(OH)_2$
3	14.7	21.4	8.4	4.2	45.9	1.0	$(Mn,Fe,Al)_5SiO_6$	79.6		

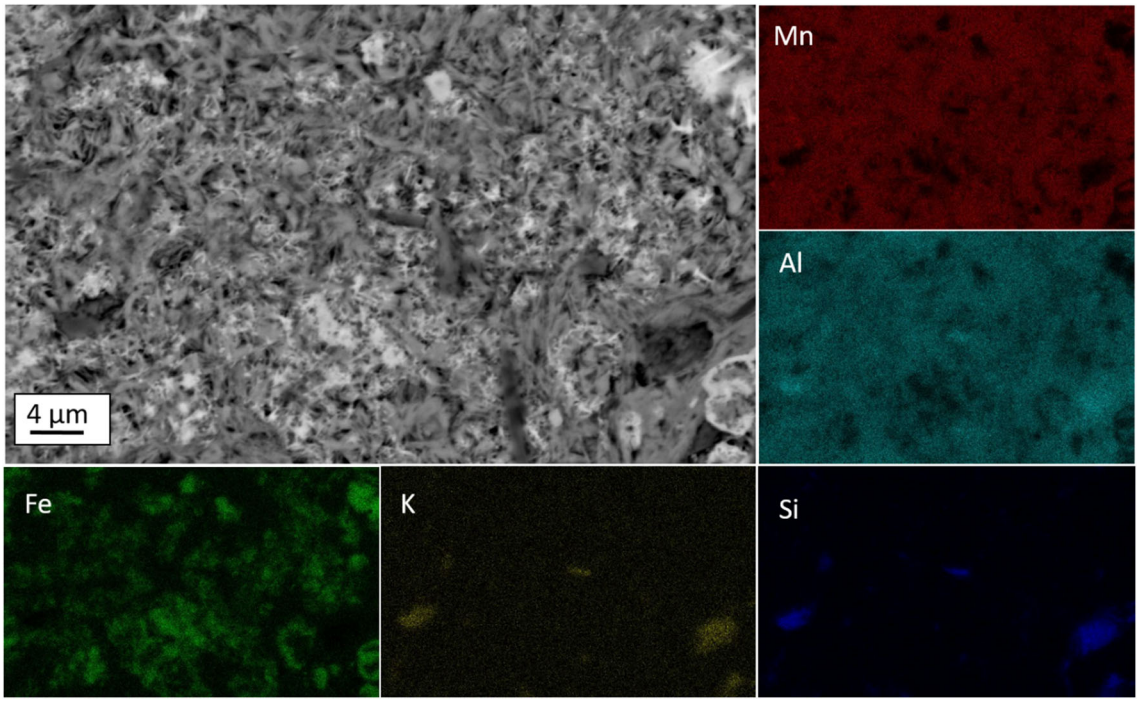

Fig. 4—Element mapping obtained by EDS of Comilog ore.

similar reduction behavior, expected reaction sequence is MnO_2-Mn_2O_3-Mn_3O_4-MnO, *i.e.* three individual steps.

3. *Analysis of reduction products*

Chemical analysis (Table III) shows an oxygen level of manganese between 1.01 and 1.05 for all non-isothermal experiments terminated at 1000 °C, *i.e.* close to MnO. As both weight and off-gas composition showed stable behavior prior to termination, it is believed that oxygen level exceeding 1.00 for these experiments is due to inaccuracy of analysis. This was supported by XRD, which showed that all major peaks were described by manganosite, which according to Rietveld analysis constituted 97 pct of the reduced ore. The remaining 3 pct were identified as quartz, kalsillite, and galaxite. The total weight loss as a function of the analyzed oxidation level of manganese (x in MnOx) is shown in Figure 7, which confirms that the weight loss behavior is representative for the reduction of higher manganese oxides to MnO in Comilog ore. A linear regression was added to visualize the relation.

Some experiments conducted with size fraction 11.20 to 15.00 mm were terminated at 550 °C, which correlated to a reduction of higher manganese oxides of 54 and 45 pct in 80 pct CO and 50 pct CO, respectively. In respect to the weight loss and rate behavior, it may be observed that these experiments were terminated close to, however prior to, the rapid increase in the reaction rate observed at temperatures 550 to 600 °C. Both samples were subjected to XRD analysis, where the mineralogy quantified by rietveld analysis is shown in Table IV. Main identified phases were tetravalent oxides and manganosite. Nsutite and lithiophorite were not detected. Only minor amounts of indermediate oxides Mn_2O_3 and Mn_3O_4 were found, which indicates that the reduction of these oxides is fast compared to reduction of MnO_2. The iron present in the ore is likely found in

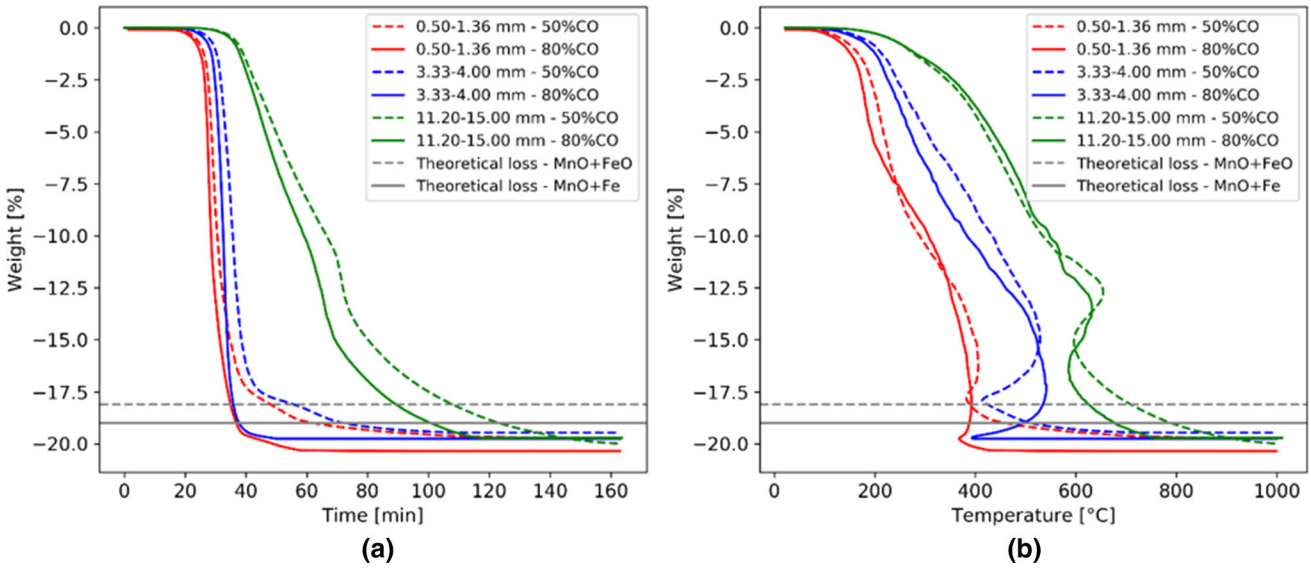

Fig. 5—Weight reduction behavior during non-isothermal (6 °C/min) reduction of Comilog ore shown as a function of (*a*) time and (*b*) sample temperature.

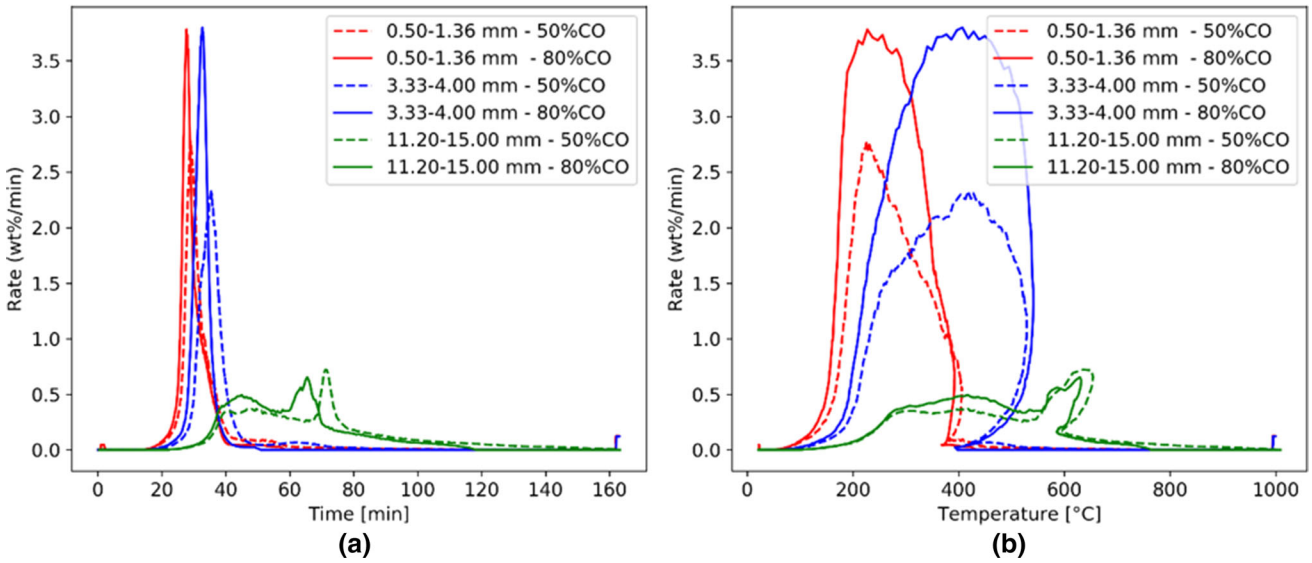

Fig. 6—Reaction rate (wt pct/min) during non-isothermal (6 °C/min) reduction of Comilog ore shown as a function of (*a*) time and (*b*) sample temperature.

solid solution in the manganese oxides. It is seen that no phases containing aluminium were identified by XRD, and it is believed that aluminium is present in solid solution in the identified manganese oxides. Prior to reduction, aluminium was found in the form of lithiophorite. Not much information is available on the thermal behavior of lithiophorite, however some studies indicate that it is subjected to dehydration at low temperatures, and is further transformed to a spinel phase, displayed as broad and weak lines in the XRD spectrum.[9,21] As such, it is suggested that the aluminium is present in the hausmannite phase.

Figure 8 shows the microstructure of a particle reduced in 80 pct CO terminated at 550 °C, where an overview including the outer edge is seen to the left and a close-up of the center is shown to the right, respectively. A disorganized structure composed of at least three distinct phases is observed. EDS analysis (Table V) showed that the bright grey phase consisted of manganese and oxygen, at a stoichiometric relation from EDS equal to $MnO_{0.6}$. Unreliable quantification of oxygen implies that the oxidation level of manganese may not be determined. Further, a medium and dark grey phase is observed, where manganese and

Table III. Chemical Analysis of Comilog Samples Exposed to Non-isothermal Reduction

Size [mm]	Pct CO	Temperature (°C)	Fe, tot	Mn, tot	MnO_2	MnO	SiO_2	Al_2O_3	K_2O	MnO*x*	RD [Pct]
0.50 to 1.36	50	1000	4.4	58.8	3.2	73.3	6.7	7.8	1.3	1.03	96
0.50 to 1.36	80	1000	4.4	59.2	0.9	75.7	6.9	7.6	1.3	1.01	99
3.33 to 4.00	50	500	3.7	59.1	24.9	56.0	3.9	6.3	1.3	1.26	72
3.33 to 4.00	50	800	3.7	60.9	9.8	70.6	4.1	6.6	1.4	1.10	89
3.33 to 4.00	50	1000	2.2	62.4	4.0	77.3	4.3	6.5	1.4	1.04	96
3.33 to 4.00	80	360	3.6	60.9	54.9	33.9	4.3	6.8	1.4	1.57	40
3.33 to 4.00	80	790	3.6	60.9	4.4	75.1	4.3	6.8	1.4	1.05	95
3.33 to 4.00	80	1000	3.2	63.5	2.4	80.0	3.9	6.2	1.3	1.02	97
11.2 to 15.0	50	550	6.2	55.2	45.1	34.5	3.1	4.9	0.8	1.52	45
11.2 to 15.0	50	1000	3.1	62.9	3.9	78.1	4.2	7.4	1.1	1.04	96
11.2 to 15.0	80	550	2.5	58.7	40.3	42.9	4.1	5.5	1.0	1.43	54
11.2 to 15.0	80	1000	2.2	64.9	5.3	79.6	4.5	6.1	0.8	1.05	95

RD = reduction degree of manganese oxides.

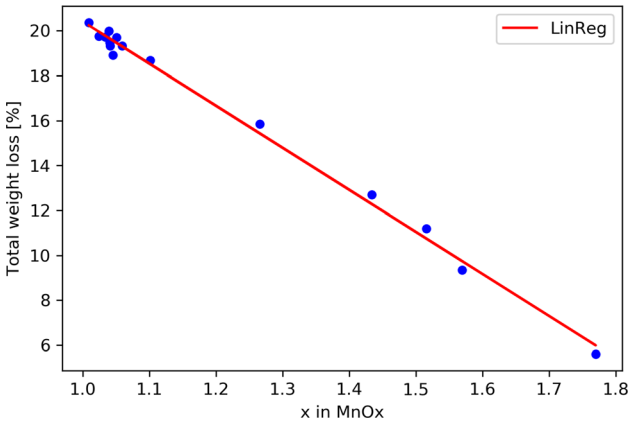

Fig. 7—Weight loss as a function of oxidation level of manganese (*x* in MnO*x*) for Comilog ore experiments.

Table IV. Quantitative Rietveld Analysis of Mineralogy in Partially Reduced Comilog Samples (11.20 to 15.00 mm)

Mineral	Formula	50 PCTCO-550 °C	80 PctCO-550 °C
Manganosite	MnO	53	58
Bixbyite	Mn_2O_3	6	7
Hausmannite	Mn_3O_4	3	3
Pyrolusite	MnO_2	33	28
Cryptomelane	KMn_8O_{16}	4	4
Quartz	SiO_2	2	—
Reduction According to Titration (MnO*x*)		45 pct	54 pct

aluminium exist in a 1:1 stochiometric relation. The phases are distinguished by the Mn/Si-ratio, being 2 and 4 in medium and dark phase, respectively. The sample obtaining a 45 pct reduction in 50 pct CO (Figure 9) exhibits a highly homogeneous structure composed of a brighter grey matrix phase with smaller regions of a darker phase dispersed throughout. The matrix phase is a MnO*x* phase, whereas the darker regions contained manganese and aluminium, present in an approximate 1:1 ratio.

11.20 to 15.00 mm particles were reduced isothermally in 50 pct CO and 70 pct CO (+ CO_2) at temperatures 400 °C to 600 °C. Samples reduced in 50 pct CO were analyzed for chemical composition, which showed that the oxygen level decreased with increasing temperature (Table VI). The analyzed MnO*x* correlates to a reduction of 36, 40, and 77 pct, for experiments held at 40 minutes at temperatures 400 °C, 500 °C, and 600 °C, respectively. The isothermal reduction products were analyzed by X-ray diffraction, where quantified mineralogy as obtained through Rietveld analysis is found in Table VII. Dehydration of nsutite appears to occur at low temperatures, converting nsutite to pyrolusite, as nsutite was not detected in any of the samples. Tetravalent oxides cryptomelane and pyrolusite are present in considerable amounts at temperatures up to and including 550 °C. In accordance with non-isothermal experiments, XRD results for isothermally reduced samples indicate a change in the removal rate of oxygen from tetravalent oxides at temperatures exceeding 550 °C. An abundance of 27 pct of cryptomelane and pyrolusite is found subsequent to 20 min reduction at 600 °C, which further showed a complete conversion after 40 min. Bixbyite were observed in minor amounts (5 pct) at temperatures 400 °C to 550 °C, whereas 30 pct were found after 20 min reduction at 600 °C.

Cross-section examinations revealed that several of the partially reduced particles appeared to follow a shrinking core mechanism. This is illustrated by the structure observed in a particle reduced in 50 pct CO at 500 °C in Figure 10, where EDS analysis showed that the particle was composed of manganese and oxygen, indicating an increasing O/Mn ratio from exterior to center of the particle. In terms of microstructure development, Comilog samples reduced isothermally and non-isothermally showed dissimilar behavior. A reaction front was observed in the former, whereas a simultaneous reduction throughout the particle appeared to occur in non-isothermal temperature

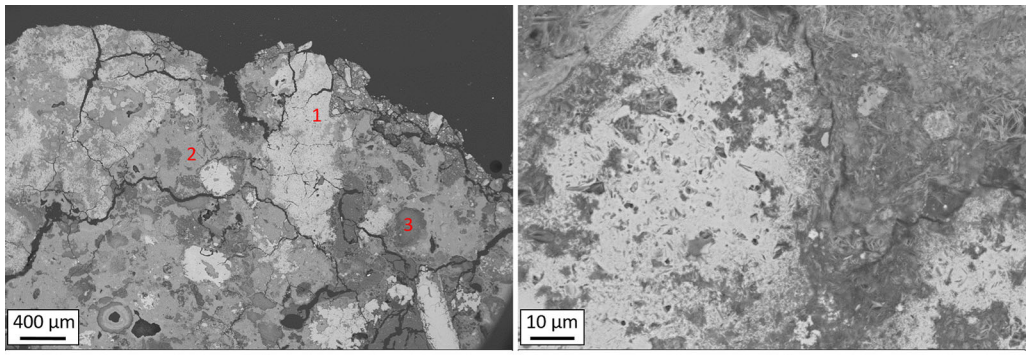

Fig. 8—Microstructure observed in Comilog ore particle (11.20 to 15.00 mm) reduced non-isothermally in 80 pctCO to 550°C. Reduction degree of 54 pct of higher manganese oxides to MnO according to chemical analysis. Overview including outer edge seen in A in scale of 400 μm, whereas B shows the center in scale 10 μm.

Table V. Chemical Composition as Analyzed by EDS [At. Pct] of Phases Observed in Microstructure of Partially Reduced Samples Shown in Figs. 8 and 9 (Average of 3 to 5 Point Analyses)

		Mn [At. Pct]	Fe [At. Pct]	Al [At. Pct]	Si [At. Pct]	K [At. Pct]	O [At. Pct]	Stochiometry from EDS	Total [Wt Pct]	Suggested Phase
80 Pct CO	bright grey (1)	59.9	—	1.7	—	—	37.3	$MnO_{0.6}$	81.0	MnO*x*
	grey (2)	22.7	1.0	19.4	4.7	—	50.7	$Mn_5Al_5SiO_{11}$	75.1	
	dark grey (3)	10.1	0.9	10.1	4.7	—	35.3	$Mn_2Al_2SiO_8$	72.7	
50 Pct CO	matrix (1)	43.1	0.4	—	—	—	56.0	$MnO_{1.3}$	85.0	MnO*x*
	minor (2)	23.4	0.3	17.3	0.9	0.1	52.9	$MnAl_{0.7}O_{2.3}$	86.0	

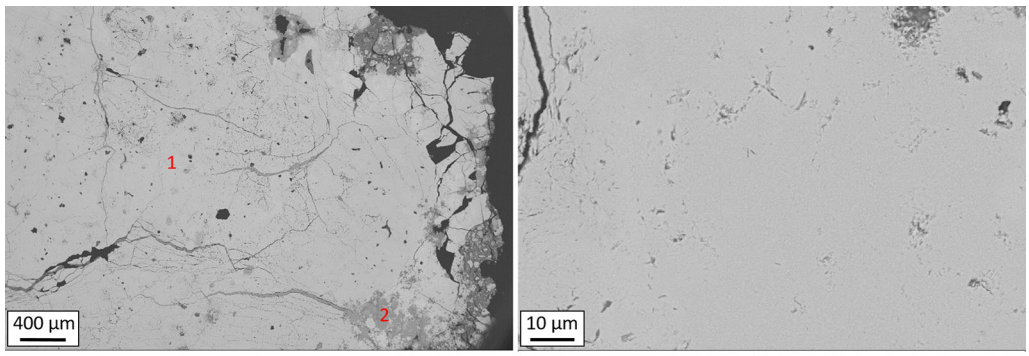

Fig. 9—Microstructure observed in Comilog ore particle (11.20 to 15.00 mm) reduced non-isothermally in 50 pctCO to 550 °C. Reduction degree of 45 pct of higher manganese oxides to MnO according to chemical analysis. Overview including outer edge seen in A in scale of 400 μm, whereas B shows the center in scale 10 μm.

regimes. A potential explanation may be that the pore structure is altered when particles are subjected to highly rapid heating rates, as the set-up used for isothermal experiments in this study subjects the particles to shock heating from ambient to target temperature, thus providing a more dense structure.

B. *Nchwaning Ore*

1. *Characterization of ore*

The chemical composition of Nchwaning ore is presented in Table I. The analyses give an oxygen level of 1.46 to 1.48, which roughly correlates to an oxidation state of Mn_2O_3. The three size fractions show highly similar composition, with a total manganese content of

Table VI. Chemical Analysis of Comilog Ore (11.20 to 15.00 mm) Reduced Isothermally in 50 PctCO-50 PctCO_2

Temperature (°C)	Holding Time [Min]	Fe, tot	Mn, tot	MnO_2	MnO	SiO_2	Al_2O_3	K_2O	MnO*x*	RD [Pct]
400	40	2.4	57.7	55.3	29.3	2.8	6.1	0.7	1.61	36
500	40	2.0	56.5	50.5	31.7	5.9	5.9	0.8	1.57	40
600	20	1.6	58.4	45.2	38.6	4.2	5.7	2.0	1.49	48
600	40	2.0	62.2	21.3	63.0	3.5	7.0	0.8	1.22	77

RD = reduction degree.

Table VII. Quantitative Rietveld Analysis of Comilog Ore Reduced Isothermally in 50 PctCO-50 PctCO_2

Mineral	Formula	400 °C (40 Min)	500 °C (20 Min)	500 °C (40 Min)	550 °C (40 Min)	600 °C (20 Min)	600 °C (40 Min)
Manganosite	MnO	24	12	29	44	28	69
Hausmannite	Mn_3O_4	21	8	16	12	14	17
Bixbyite	Mn_2O_3	5	5	5	5	30	13
Pyrolusite	MnO_2	37	66	39	5	7	—
Cryptomelane	KMn_8O_{16}	9	8	2	32	20	—
Quartz	SiO_2	4	2	9	3	1	1
MnO*x* from Titration		36 pct reduction		40 pct reduction		48 pct reduction	77 pct reduction

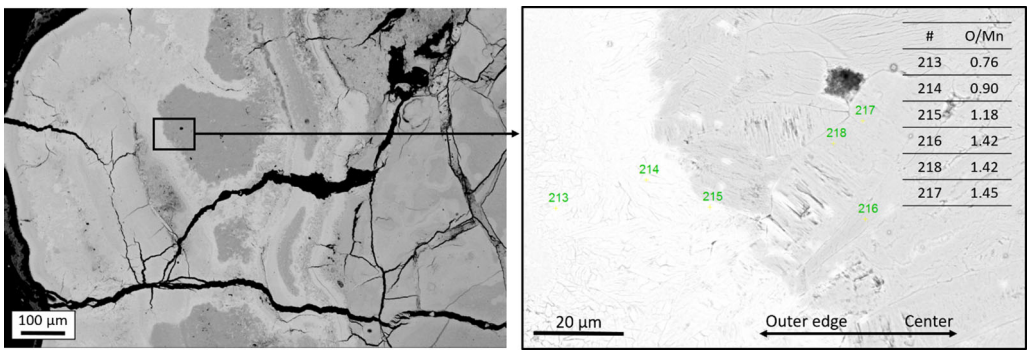

Fig. 10—Cross-section examination of Comilog particle reduced 40 pct isothermally at 500°C (40 min) in 50 pct CO.

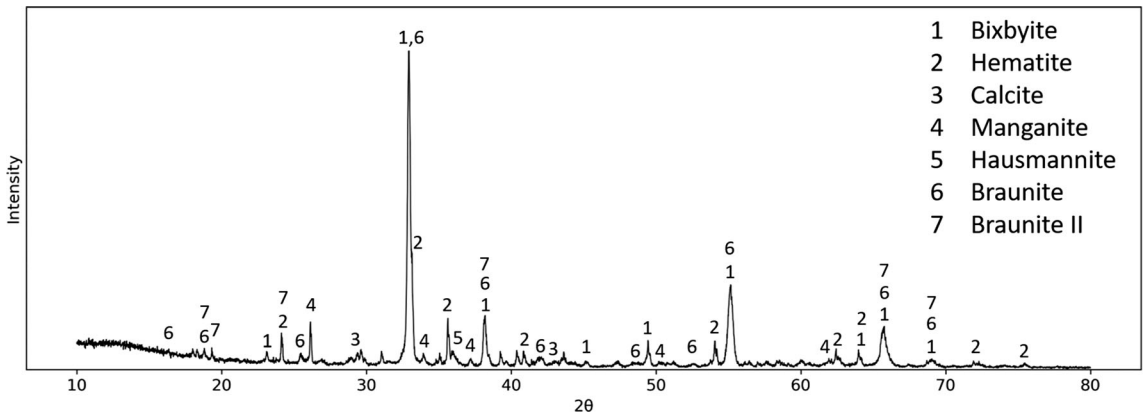

Fig. 11—XRD spectrum with identified phases for Nchwaning ore (11.20 to 15.00 mm).

46 pct and iron content of 10 pct. CaO and SiO_2 are present at concentrations 6 to 7 pct, whereas only minor amounts of MgO is found. The obtained XRD spectrum for Nchwaning ore in size fraction 11.20 to 15.00 mm is shown in Figure 11. XRD indicated that bixbyite, braunite, and braunite II were the main Mn-bearing minerals in Nchwaning ore. Further, hematite, calcite, and manganite appeared to be present in considerable concentrations. Several low intensity peaks were observed, correlating to phases of minor abundance. Suggested phases are hausmannite, johannesite, kutnohorite, (Ca,Mg)-silicate, as well as $AlFe_2O_4$. The abundance was quantified through Rietveld analysis using TOPAS 5, where the obtained quantified mineralogy for all three size fractions is found in Table VIII. Only minor concentrations of braunite and braunite II were found, whereas bixbyite was determined as the main constituting phase of ca. 60 pct.

Cross-section examinations revealed that the microstructures found in Nchwaning ore were mainly of two distinct types, *i.e.* particles rich in braunite and carbonate (type 1), and particles rich braunite II (type 2). The observed microstructures can be observed in Figure 12. The dark grey phase in type 1 is a carbonate phase, which is mainly calcite. However, a varying concentration of magnesium in the carbonate was observed by EDS point analysis. The brighter grey phase is identified as braunite, whereas some areas correspond to hematite. Particle type 2 appeared relatively homogeneous in light microscope and SEM, where the constituting phase was identified as braunite II. Nonetheless, element mapping, as well as point analysis, showed that the concentrations of manganese, iron, silicon and calcium varies throughout the structure.

Some of the braunite II particles contained minor amounts of hematite and calcite. The microstructure, with identified phases, of one of these particles is shown in Figure 13. EDS indicated that the matrix phase was braunite II in two different modifications distinguished by the Mn/Fe ratio. Calcite and hematite, both containing small amounts of manganese, can be seen throughout the structure. Chemical composition obtained by EDS of the observed phases is presented in Table IX. As braunite and braunite II was determined as the potential matrix phases by EDS, it is believed that these minerals were wrongfully quantified as bixbyite by the Rietveld refinement, as bixbyite, braunite, and braunite II have similar XRD patterns. A similar disagreement between XRD and SEM/EDS was also observed by Sørensen et al. in the case of Wessels ore.[7] If one does not differentiate between bixbyite, braunite I, and braunite II, the obtained mineralogy shows high correlation with the reported mineralogy of Nchwaning ore by Visser *et al.*[6].

Table VIII. Quantitative Rietveld Analysis of Nchwaning Ore

Mineral	Formula	0.50 to 1.36 mm	3.33 to 4.00 mm	11.20 to 15.00 mm
Bixbyite	$(Mn,Fe)_2O_3$	61	61	56
Hematite	Fe_2O_3	10	10	16
Calcite	$CaCO_3$	9	11	7
Braunite I	Mn_7SiO_{12}	6	4	6
Braunite II	$CaMn_{14}SiO_{24}$	3	4	5
Hausmannite	Mn_3O_4	4	3	< 1
Manganite	MnO(OH)	7	7	8

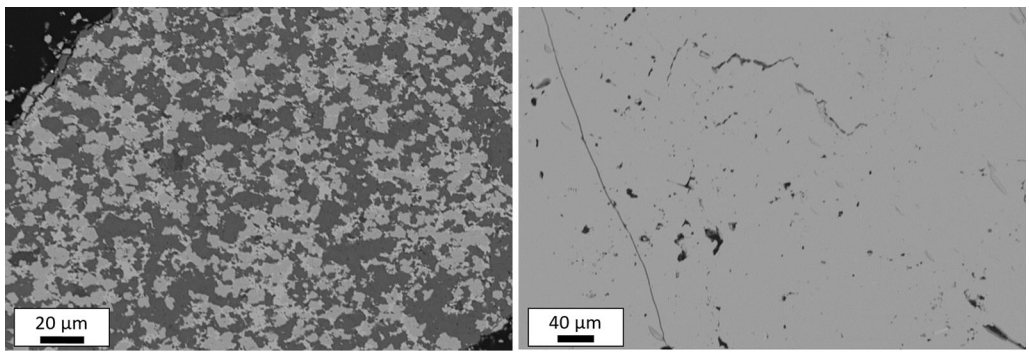

Fig. 12—Microstructure of the two main types of structures observed in Nchwaning ore seen in (*a*) and (*b*), respectively.

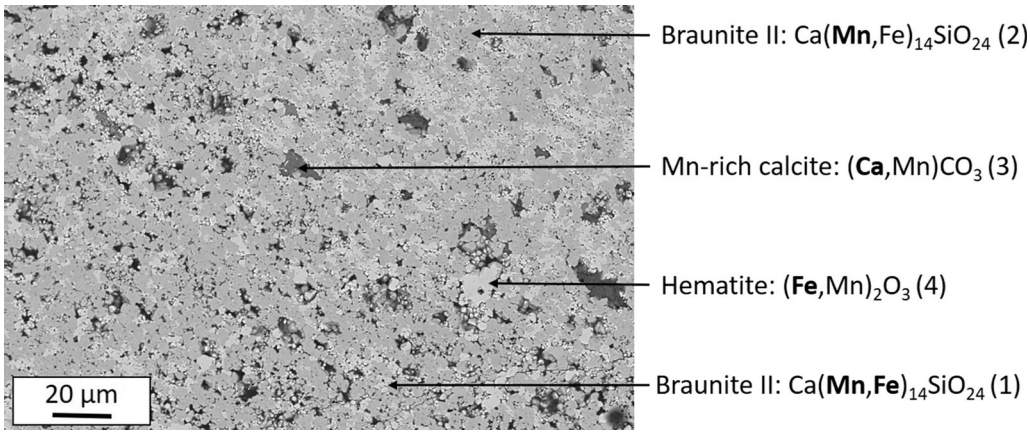

Fig. 13—Microstructure of Nchwaning ore (11.20 to 15.00 mm) obtained by backscatter imaging. Phases numbering correlate to chemical compositions shown in Table IX.

Table IX. Chemical Composition of Phases in Nchwaning Ore (11.20 to 15.00 mm) According to EDS Point Analysis

	Values from EDS								Proposed Phase	
	Mn [At. Pct]	Fe [At. Pct]	Si [At. Pct]	Ca [At. Pct]	O [At. Pct]	C [At. Pct]	Stoichiometry from EDS	Total [Wt Pct]	Mineral	Stochiometry
1	29.8	16.2	3.3	1.0	46.0	3.8	$(Mn,Fe)_{14}CaSiO_{14}$	83.8	Braunite II	$Ca(Mn,Fe)_{14}SiO_{24}$
2	39.2	2.4	5.9	3.3	48.9	—	$(Mn,Fe)_{12}CaSi_2O_{15}$	82.3	Braunite II	$Ca(Mn,Fe)_{14}SiO_{24}$
3	4.1	—	—	31.6	49.6	13.7	$(\mathbf{Ca},Mn)_3CO_4$	76.8	Carbonate	$(Ca,Mn)CO_3$
4	3.7	50.4	—	—	41.3	—	$(Mn,\mathbf{Fe})O_{0.8}$	90.0	Hematite	$(Fe,Mn)_2O_3$

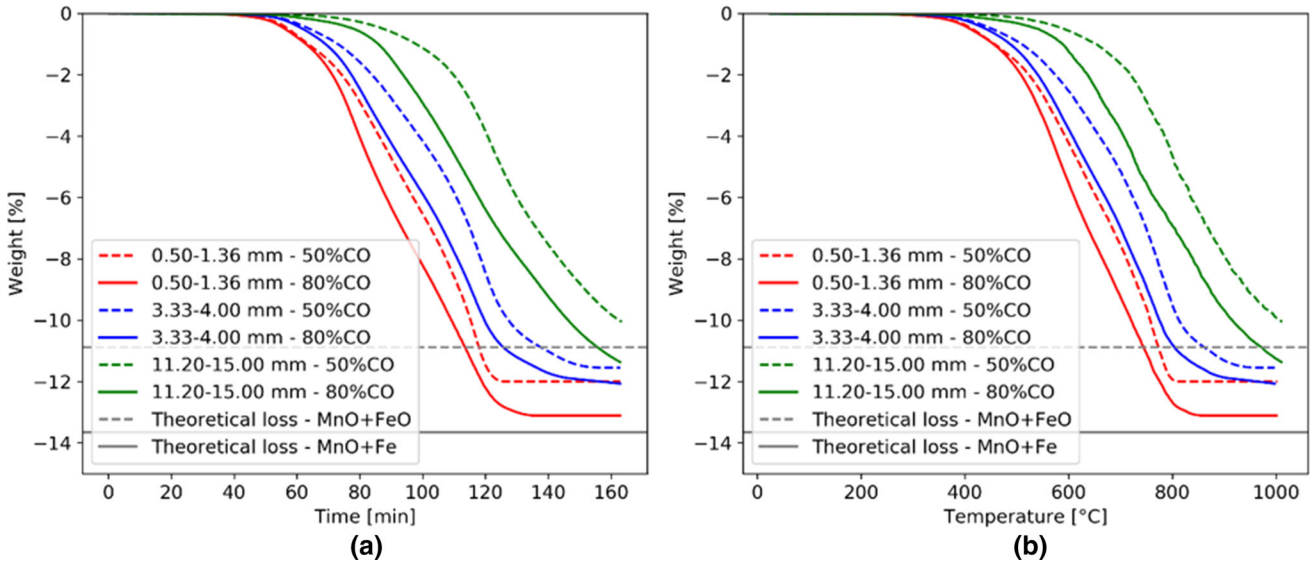

Fig. 14—Weight reduction behavior during non-isothermal (6 °C/min) reduction of Nchwaning ore as a function of *a*: time and *b*: sample temperature.

2. *Weight reduction behavior*

Non-isothermal weight reduction behavior of Nchwaning ore, as seen in Figure 14, is similar when presented as a function of temperature and time, respectively. In contrast to Comilog ore, Nchwaning ore follows the furnace temperature. The reaction rates (Figure 15) were calculated from the weight change at every 2-minute interval, where it was observed that all characteristics present at shorter periods were conserved. For particle size 0.50 to 1.36 mm, the recorded

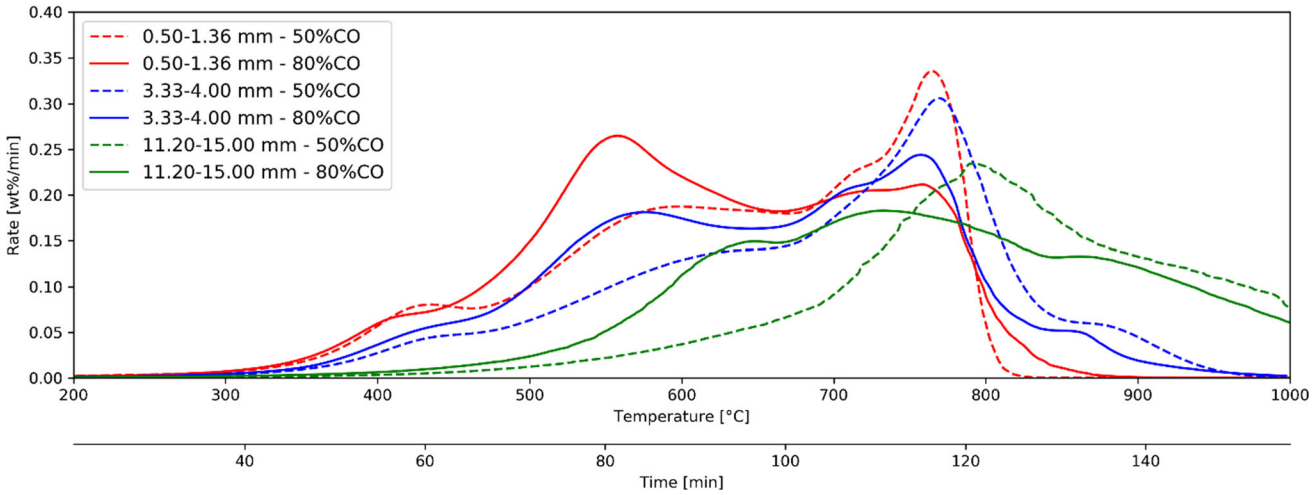

Fig. 15—Reaction rate (wt pct/min) during non-isothermal (6 °C/min) reduction of Nchwaning ore.

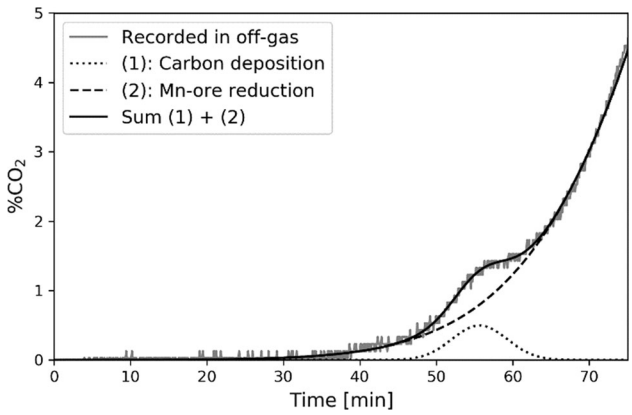

Fig. 16—Separation of $pctCO_2$ correlating to reverse Boudouard reaction and manganese ore reduction by Gaussian fitting function. Curves are valid for Nchwaning ore (0.50 to 1.36 mm) reduced in 80 pctCO-20 $pctCO_2$.

$pctCO_2$ in the off-gas decreased below set-point at temperatures exceeding 800 °C and 870 °C for 50 pctCO and 80 pctCO, respectively. $pctCO_2$ was adjusted to zero in these cases, resulting in a stable weight in Figure 14. The "negative" CO_2-concentration suggests the occurrence of the Boudouard reaction ($2CO = C + CO_2$), potentially accompanied by carbon deposition (from reverse Boudouard reaction) at lower temperatures. The rate of particle size 0.50 to 1.36 mm reduced in 50 pctCO started to increase at ca. 280 °C. At 380 to 410 °C, the rate increased with a steeper slope, followed by a plateau. It is believed that this minor peak is due to the left shifted Boudouard reaction, causing carbon deposition. Furnace calibration experiments with quartz showed that the left and right shifted Boudouard reaction occurred at similar temperature ranges when quartz was used as the sample material. This indicates that the Boudouard reaction was not catalyzed by the iron oxides in Nchwaning ore.

It is believed that the initial peak observed in the reaction rate curves of Nchwaning ore, located at temperatures close to 400 °C, is due to carbon deposition. The extent of carbon deposition was estimated by using a Gaussian fitting function to the recorded CO_2 in the off-gas. The resulting separation of the CO_2 produced from the reverse Boudouard reaction and ore reduction, respectively, is presented in Figure 16 for size fraction 0.50 to 1.36 mm reduced in 80 pctCO-20 $pctCO_2$. Estimated amount of deposited carbon is below 0.4 g for all experiments, which correlates to a maximum of 3.6 pct of total weight loss. Figure 17 shows the reaction rate curves, where the contribution of reverse Boudouard reaction has been omitted.

The reduction is slowly initiated at approximately 250 °C for particle size 0.50 to 1.36 mm and 3.33 to 4.00 mm, whereas a sample temperature of 400 °C is required to initiate reduction of size 11.20 to 15.00 mm. The reaction rate curves (wt pct/min) indicate that the reduction of Nchwaning ore occurs through multiple steps, as several peaks are observed. The two smaller particle size fractions show highly similar rate behavior, where two distinct peaks in the rate are observed, at temperatures 580 °C and 780 °C, respectively. The majority of the weight loss experienced by Nchwaning ore is due to reduction of Mn_2O_3-oxides and reduction of iron oxides, which both may proceed through several stable intermediate oxides. In addition to the two main peaks, a change in the rate behavior is observed at temperatures between 800 °C and 900 °C. This is believed to be due to carbonate decomposition.

3. *Analysis of reduction products*

Chemical analysis showed that all non-isothermal experimental runs resulted in a complete reduction of higher manganese oxides to MnO at 1000 °C, except for the largest size fraction (11.20 to 15.00 mm) reduced in 50 pctCO-50 $pctCO_2$ (Table X). XRD showed that fully

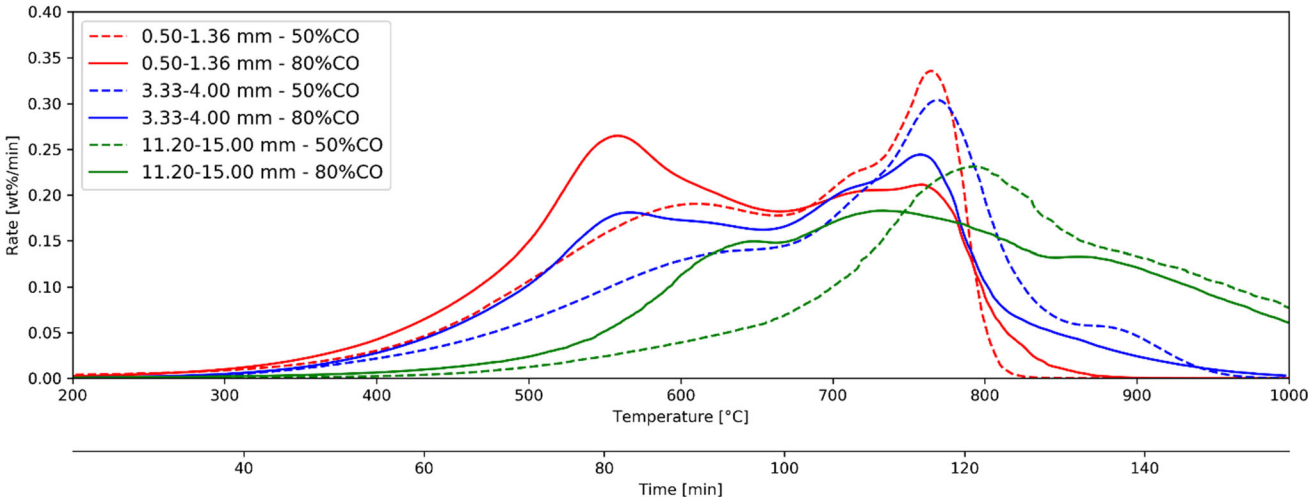

Fig. 17—Reaction rate curves (wt pct/min) for non-isothermal (6 °C/min) reduction of Nchwaning ore excluding effect of reverse Boudouard reaction.

Table X. Chemical Analysis of Nchwaning Samples Exposed to Non-isothermal Reduction

Size [mm]	PctCO	Temp. [°C]	Fe, tot [Wt Pct]	Mn, tot [Wt Pct]	MnO_2 [Wt Pct]	MnO [Wt Pct]	SiO_2 [Wt Pct]	CaO [Wt Pct]	MgO [Wt Pct]	CO_2 [Wt Pct]	MnO*x*	RD
0.5 to 1.36	50	1000	11.3	52.4	0.05	67.6	6.9	6.9	1.1	—	1.00	100
0.5 to 1.36	80	1000	11.4	53.7	0.05	67.9	7.1	7.0	1.1	—	1.00	100
3.33 to 4.00	50	300	10.5	46.2	34.1	31.9	5.7	6.3	1.0	—	1.47	0
3.33 to 4.00	50	800	11.0	50.5	0.05	65.1	6.6	6.6	1.1	—	1.00	100
3.33 to 4.00	50	1000	11.6	52.0	0.05	67.1	6.9	6.8	1.1	—	1.00	100
3.33 to 4.00	80	800	10.4	51.2	0.05	66.1	6.9	7.2	1.1	—	1.00	100
3.33 to 4.00	80	1000	11.4	52.6	0.05	67.9	7.4	6.7	1.0	—	1.00	100
11.2 to 15.00	50	800	7.6	47.5	17.0	47.5	7.2	9.8	2.5	4.0	1.23	52
11.2 to 15.00	50	1000	7.6	53.1	6.5	63.3	7.6	7.8	1.4	—	1.08	84
11.2 to 15.00	80	816	7.2	51.3	16.7	52.6	6.9	7.9	0.4	3.9	1.21	56
11.2 to 15.00	80	1000	13.5	47.7	0.05	61.6	7.8	7.4	1.9	—	1.00	100

RD = reduction degree of manganese oxides.

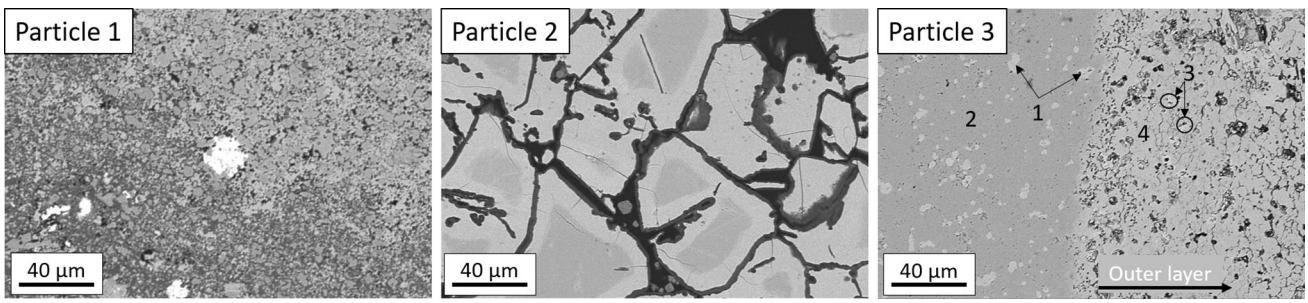

Fig. 18—Microstructure observed in three separate particles (11.20 to 15.00 mm) reduced non-isothermally in 80 pctCO to 800 °C. Reduction degree of 55 pct of higher manganese oxides to MnO according to chemical analysis.

reduced samples mainly consisted of a monoxide phase, where cations were a combination of manganese, iron, and calcium. Identification of minor abundance phases is less reliable, however, proposed phases are braunite II/bixbyite, $(Ca,Fe)SiO_4$, Ca_3SiO, hematite, and wüstite.

Partially reduced samples were cut to expose the cross-section and investigated in SEM, which revealed large variations in microstructure between particles exposed to similar experimental conditions. Figure 18 shows the microstructure of three 11.20 to 15.00 mm particles reduced in 80 pctCO. The experiment was

terminated at 800 °C, which according to chemical analysis resulted in a 55 pct reduction of higher manganese oxides to MnO. Particle 1 exhibited a heterogeneous structure, where a bright and darker grey phase coexisted at apparent random distribution throughout the particle. Minor abundance of a white phase was also observed, which according to EDS contained manganese, barium, titanium, and sulphur, all in an approximate 1:1 ratio. Particle 2 appeared to have been subjected to a high degree of disintegration during heating and reduction. Individual grains were observed, where a thin rim of $(Mn,Fe,Ca)_2SiO_3$ surrounded each of the grains. Within the majority of the individual grains, a distinction between the core and the outer layer was observed. EDS analysis indicated that both regions correlated to braunite II, deduced from the relation between Ca, Si, and (Mn + Fe). The oxygen to manganese and iron ratio was approximately 1.3 in the center, whereas a ratio of 1.0 was found in the outer region. Black areas observed between the grains are epoxy. A product layer appeared to have been formed in particle 3, which is seen to the right. Both the center and the exterior were composed of two individual phases with a darker grey matrix phase and a brighter grey phase dispersed throughout. A higher degree of heterogeneity was observed in the product layer, as well as a higher porosity. EDS analysis indicated that the matrix was a braunite phase, and brighter grey areas were observed to be a (Mn,Fe)xOy-oxide. The difference between the center and exterior phases was within the iron concentration, as can be seen in Table XI.

11.20 to 15.00 mm particles reduced in 50 pctCO non-isothermally up to 800 °C obtained a reduction degree of 51 pct. The cross-section microstructure observed in two individual particles show dissimilar microstructure (Figure 19), where the two structures are highly similar to the two main structures observed in untreated ore (Figure 12). Common for both is the lack of topochemical reaction pattern. Both particles exhibited a relatively homogeneous structure, where the matrix phase of particle 1 showed only minor differences relative to the analyzed composition of braunite in Nchwaning ore. A brighter grey phase is dispersed throughout, which was depleted of calcium and silicon. For particle 2, a clear distinction of a dark and bright grey phase is observed. Investigations at higher resolution showed that the dark phase was composed of two individual phases, both of which contained mainly calcium and magnesium. It is believed that the two phases are $CaCO_3$ and $(Ca,Mg)CO_3$, where an approximate 1:1 ratio was measured by EDS for calcium and magnesium in the latter. The bright phase showed composition correlating to braunite. Metallic iron was not detected by SEM/EDS in any of the investigated particles obtained from non-isothermal reduction experiments, indicating that the conditions were not sufficient to produce metallic iron. The samples were also subjected to XRD analysis, which showed that the main constituting minerals were bixbyite (potential partially braunite and/or braunite II) and monoxide. Quantified results as obtained by TOPAS are shown in Table XII. This implies that, if present at all, hausmannite is only present in minor concentrations. This indicates that the

Table XI. EDS Analysis (At. Pct) of Partially Reduced Nchwaning Particle (11.20 to 15.00 mm) Correlating to Particle 3 in Fig. 18

Location	#	Mn [At Pct]	Fe [At Pct]	Si [At Pct]	Ca [At Pct]	O [At. Pct]	Stochiometry from EDS	Total [Wt Pct]	Suggested Phase
Center	1	3.3	45.6	—	—	50.7	(Fe,Mn)O	94.4	—
	2	41.1	—	5.7	—	51.7	$(Mn,Fe)_7SiO_9$	86.6	Braunite
Product Layer	3	31.7	20.8	—	—	46.0	$(Mn,Fe)O_{0.9}$	87.4	—
	4	37.1	10.4	6.0	—	46.3	$(Mn,Fe)_8SiO_8$	87.8	Braunite

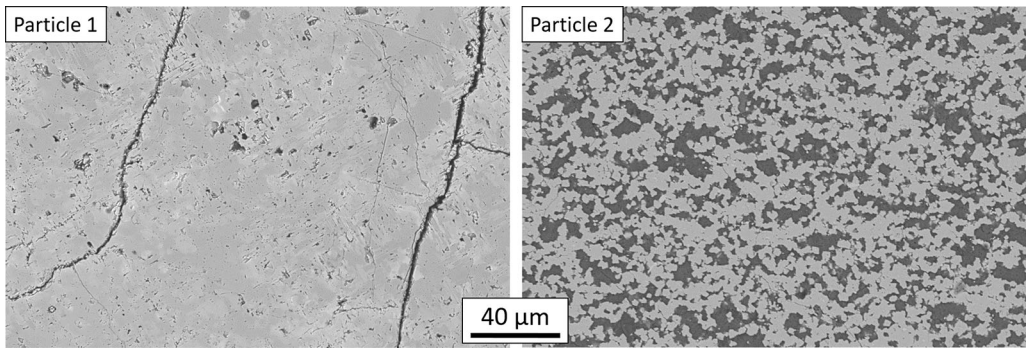

Fig. 19—Microstructure observed in two separate particles (11.20 to 15.00 mm) reduced non-isothermally in 50 pctCO to 800 °C. Reduction degree of 51 pct of higher manganese oxides to MnO according to chemical analysis.

Table XII. Quantitative Rietveld Analysis of Mineralogy in Partially Reduced Nchwaning Samples (11.20 to 15.00 mm)

Mineral	Formula	80 pct CO-816°C (55 Pct Reduction)	50 pct CO-800°C (51 Pct Reduction)
Bixbyite	$(Mn,Fe)_2O_3$	29	26
Monoxide	(Mn,Fe)O	47	42
Calcite	$(Ca,Mg)CO_3$	10	21
Braunite	Mn_7SiO_{12}	5	4
Braunite II	$CaMn_{14}SiO_{24}$	4	3
Hematite	Fe_2O_3	2	2
Wüstite	FeO	3	2

Table XIII. Chemical Analysis of Isothermal Nchwaning Reduction Products. 11.20-15.00 mm Particles Reduced in 50 PctCO-50 PctCO_2

Temperature (°C)	Time (Min)	Fe, Tot	Mn, Tot	MnO_2	MnO	SiO_2	CaO	MgO	CO_2		RD
600	60	20.2	41.6	16.6	40.1	3.7	5.8	1.0	0.5	1.25	47
700	60	6.3	52.0	26.5	45.5	5.2	5.9	1.8	4.2	1.32	
800	60	10.6	44.2	13.0	46.5	7.1	9.4	2.9	4.5	1.19	
900	30	13.3	47.4	8.7	54.1	6.8	5.8	1.9	1.5	1.12	75

reduction of hausmannite to manganosite is rapid, implying that the overall reduction of Mn_2O_3 to MnO may be considered as a single-step reduction. Further, considerable concentrations of calcite were detected, showing that carbonates have not been decomposed at 800 °C. This correlates with the reaction rate behavior, where it was suggested that carbonates were decomposed between 800 °C and 900 °C. Iron may be present in the form of hematite and wüstite, however the abundance of iron oxides in the sample is insufficient to conclude.

11.20 to 15.00 mm particles were reduced isothermally in 50 and 70 pctCO at temperatures 600 to 900 °C. Chemical analysis of the samples reduced 50 pctCO showed a 47 pct reduction of higher manganese oxides after 60 minutes reduction at 600 °C, whereas a 75 pct reduction was obtained after 30 minutes at 900 °C (Table XIII). In accordance with results from non-isothermal experiments, hausmannite was not detected by XRD in any of the isothermally reduced samples (Table XIV). Bixbyite and monoxide were the identified Mn-bearing minerals at all temperatures. Iron was found in the form of hematite and wüstite. The reduction of iron oxides to metallic iron will be dependent on temperature, oxygen pressure, and the activity of iron. According to thermodynamics, metallic iron is the stable iron phase when reduced in 80 pctCO-20 pctCO_2 at 1000°C in an ideal system. However, as the activity of iron in the manganese ore is expected to be lower compared to an ideal system and the evaluated gas composition lies close to the phase boundary of wüstite, it is assumed that the conditions are not sufficient in order to obtain a complete reduction to metallic iron. Metallic iron was not detected by XRD or SEM/EDS investigations of both partly and fully reduced samples, supporting that the reduction of hematite subsides with the formation of wüstite. Further, hematite and wüstite were the only observed oxidation states of iron, indicating that the reduction of intermediate oxide magnetite (Fe_3O_4) is fast.

No correlation between phases and distance from surface was observed by investigations in SEM, implying that a topochemical reaction pattern was not observed. Nonetheless, dissimilarities were observed between microstructures obtained during reduction in 50 pct CO and 70 pct CO (Figure 20). Samples reduced in 50 pct CO showed braunite in coexistence with hematite at all temperatures, implying that no reduction products were observed. Identification of hematite was performed through comparison of composition of hematite in untreated ore. The microstructure of samples reduced in 70 pct CO showed two distinct phases co-existing, where the dark grey phase appeared to become more dominant with increasing temperature. EDS analysis showed that the bright grey phase exhibit a composition highly similar to braunite identified in untreated ore, however depleted in calcium. All calcium and magnesium present in the samples were detected in the dark grey phase, at concentrations up to 28 at. pct and 16 at. pct, respectively. The analyzed carbon content were 1 to 2 at. pct in the bright phase and 5 to 7 at. pct in the dark phase, which may indicate that the dark phase is a carbonate rather than monoxide. Nonetheless, the variance may also be due to varying thickness of carbon coating. Overall, the trends observed in the microstructures show high correlation with the microstructures found in untreated ore, as was seen in Figure 12. Metallic iron was not observed in any of the investigated samples.

C. *Observations*

Non-isothermal reduction of Comilog ore in particle size range 0.50 to 4.00 and 3.33 to 4.00 mm is observed to occur simultaneously throughout the particle, where the reduction is observed as a single-step in the

Table XIV. Quantitative Rietveld Analysis of Isothermally Reduced Nchwaning Ore (11.20 to 15.00 mm) in 50 pctCO-50 pctCO_2

Mineral	Formula	600°C (60 Min)	700°C (60 Min)	800°C (60 Min)	900°C (30 Min)
Monoxide	(Mn,Fe)O	27	32	36	58
Bixbyite	$(Mn,Fe)_2O_3$	44	47	41	25
Hematite	Fe_2O_3	14	2	6	4
Magnetite	Fe_3O_4	3	—	—	—
Wüstite	FeO	9	—	9	3
Calcite	$(Ca,Mg)CO_3$	4	8	8	7
MnO*x* from Titration		47 pct reduction			75 pct reduction

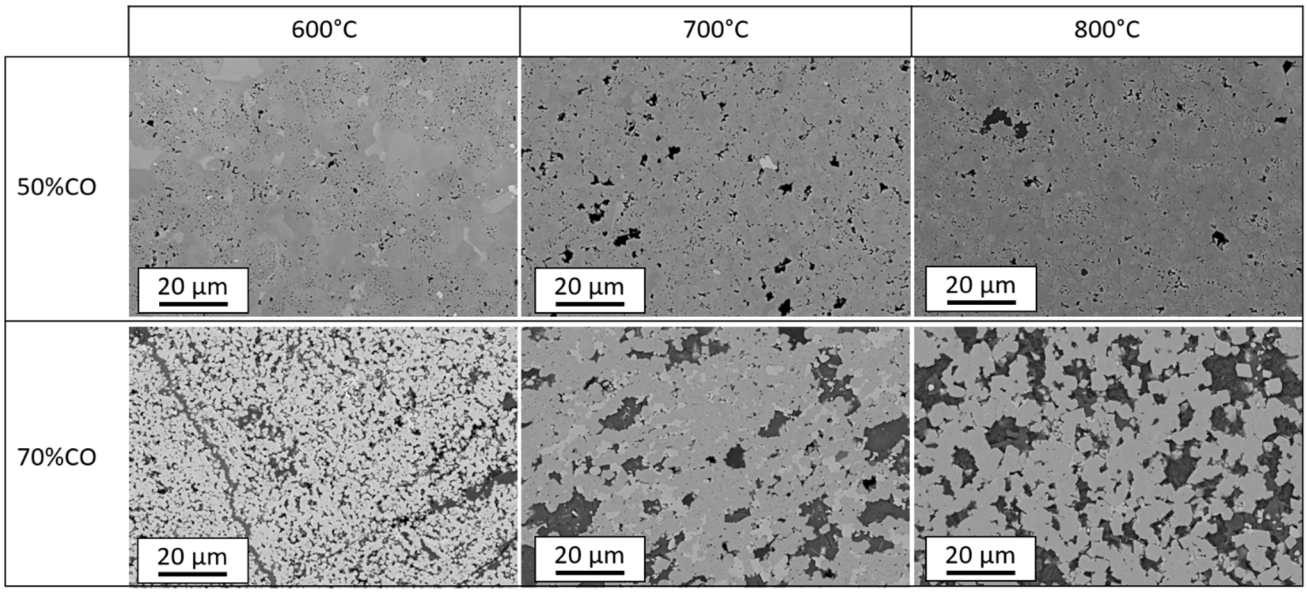

Fig. 20—Microstructure of isothermal reduction products (center view). Scale bar reads 20 μm.

thermogravimetric data. Isothermal and non-isothermal reduction, respectively, of particle size 11.20 to 15.00 mm show high correlation, where the reduction proceeds through two distinct stages. The first stage occurred at temperature range 200 to 550°C, where MnO_2 was partially reduced to MnO. The intermediate oxidation states, Mn_2O_3 and Mn_3O_4, were not detected, implying that MnO_2 reduce to MnO in a single step. The second stage was initiated at temperature range 550 to 580°C, where the reaction rate was observed to increase rapidly. According to XRD analyses, this behavior was caused by the rapid decomposition of remaining MnO_2, which formed Mn_2O_3. The Mn_2O_3 continued to reduce to MnO. The rapid removal resulted in a heat production, which provided an additional driving force for the remaining reduction. It may be suggested that the decomposition temperature of pyrolusite to bixbyite is close to 550°C. Some discrepancy was observed in the microstructure development during isothermal and non-isothermal reduction. The majority of the investigated particles showed no indications of a topochemical reaction mechanism, however some isothermally reduced particles showed a clear shrinking core pattern. It is suggested that the rapid temperature development (shock heating) experienced during the isothermal set-up alters the pore structure in the particles, resulting in a denser particle surface. It may also be due to the lower reaction temperature.

Analysis indicates that the overall reduction of Nchwaning ore is a two-step reduction, *i.e.* Mn_2O_3 to MnO and Fe_2O_3 to FeO. Insignificant concentrations of the potential intermediate oxidation states hausmannite (Mn_3O_4) and magnetite (Fe_3O_4) was found. This is in high correlation with the calculated reduction rate behavior, which showed two distinct peaks. The weight reduction behavior showed that the reduction was still ongoing in particle size 3.33 to 4.00 mm at 800°C. Chemical analysis showed that all higher manganese oxides were reduced to MnO at this temperature (MnO*x*, $x = 1.00$). This indicates that the reduction of manganese oxides is initiated prior to iron oxides in Nchwaning ore. No evidence of a reaction front was observed through investigation of microstructure development in partially reduced samples. The reduction

rather appeared to occur simultaneously throughout the particle in both isothermal and non-isothermal temperature regimes.

Comilog ore is found to reduce at a lower temperature range compared to Nchwaning ore. Furthermore, it was observed that while Nchwaning ore largely follows the furnace temperature, the temperatures of Comilog ore is largely affected by the exothermic reactions. This is both due to the higher oxidation level of Comilog ore compared to Nchwaning ore, but also due to the faster reduction rate obtained for MnO_2 to MnO in Comilog ore compared to Mn_2O_3 to MnO in Nchwaning ore. Comilog ore obtained a complete prereduction to MnO at 800°C for particle sizes 0.50 to 15.00 mm, which implies that it will not produce any CO_2 that may be consumed by the Boudouard reaction in an industrial furnace. A nearly completed prereduction was obtained for Nchwaning ore in particle size 0.50 to 4.00 mm at 800°C.

The microstructures observed in Comilog ore showed a high variety, and no clear categories were found. Nchwaning ore was found exhibit two main microstructure types. Partially reduced samples also showed a large variance in the microstructure, however the structure appearance does not indicate that the ores will reduce topochemically in an industrial furnace. Nonetheless, the reduction do likely not proceed uniformly throughout the particle, as a decreasing particle size had a promoting effect on the reduction rate of both ores. Previous studies have also observed that Comilog and Nchwaning ore reduce faster in CO–CO_2 atmospheres in smaller particle sizes.[2,16,22] Gao[11] observed no effect by changing the particle size between < 45 to 1000 μm when reducing a precalcined ore in CO-CO_2 atmosphere. This may suggest that the ores have a threshold value at which the kinetics are affected by the particle size. Further, an increasing CO-concentration also had a promoting effect on the reaction rate for both ores. An increased content of CO correlates to a lower oxygen pressure, which in turn correlates to a higher driving force of reduction. A promoting effect of CO has also been found by previous researchers.[5,11]

IV. CONCLUSION

The reduction of Comilog and Nchwaning manganese ores was investigated in isothermal and non-isothermal temperature regimes in CO-CO_2 atmosphere. The results were evaluated through thermogravimetric curves, chemical composition, XRD, and SEM analyses.

Comilog ore was found to be constituted by various MnO_2-minerals, including cryptomelane, nsutite, and pyrolusite. At temperatures below 550 to 580 °C, these MnO_2 oxides were reduced to MnO in an overall single step. At temperatures 550 to 600°C, any present MnO_2 was subjected to rapid conversion. The minerals formed bixbyite(Mn_2O_3) upon the rapid reduction, which continued to reduce to MnO. Manganosite was the main reduction product at all evaluated temperatures and holding times. It is believed that a more dense structure is formed when the ore is subjected to isothermal heating, as a reaction front was observed. This was not observed in any non-isothermal experiments.

Nchwaning ore was found to be mainly constituted by Mn_2O_3-oxides (braunite, braunite II and bixbyite), calcite and hematite. Two distinct particle types were observed, *i.e.* particles rich in braunite and carbonate, and particles rich in braunite II, respectively. Manganese and iron oxides reduce at highly similar temperature ranges, however the manganese oxide reduction was initiated prior to iron oxides in smaller particle sizes (< 4 mm). Reduction of trivalent oxides to MnO appeared to be a single-step reaction, as the intermediate oxide hausmannite was not detected. The reduction of trivalent oxides was initiated at 280 °C to 400 °C, depending on particle size. Investigations of microstructure showed no indications of a topochemical reaction mechanism.

ACKNOWLEDGMENTS

This publication has been funded by HighEFF - Centre for an Energy Efficient and Competitive Industry for the Future, an 8-year Research Centre under the FME-scheme (Centre for Environment-friendly Energy Research, 257632). The authors gratefully acknowledge the financial support from the Research Council of Norway and user partners of HighEFF, particularly those a member of the Norwegian Ferroalloy Producers Research Association (FFF).

FUNDING

Open Access funding provided by NTNU Norwegian University of Science and Technology (incl St. Olavs Hospital - Trondheim University Hospital).

REFERENCES

1. J. Kaczorowski, T. Lindstad, and M. Syvertsen: *ISIJ international*, 2007, vol. 47, pp. 1599–1604.

2. R.J. Ishak: Dr. Ing thesis, NTNU, 2002.
3. M. Tangstad, P. Calvert, H. Brun, and A.G. Lindseth: in *Proceedings: Tenth International Ferroalloys Congress*, vol. 1, 2004, p. 4.
4. R. Kononov, O. Ostrovski, and S. Ganguly: *ISIJ international*, 2009, vol. 49, pp. 1099–1106.
5. K.L. Berg: The Norwegian University of Science and Technology, 1998.
6. M. Visser, H. Smith, E. Ringdalen, and M. Tangstad: in *The thirteenth International Ferroalloys Congress, INFACON XIII*, Kazakhstan, 2013.
7. B. Sorensen, S. Gaal, E. Ringdalen, M. Tangstad, R. Kononov, and O. Ostrovski: *Int. J. Miner. Process.*, 2010, vol. 94, pp. 101–10.
8. I.M. Varentsov and G. Grasselly: *Methods, Vol. IE Schweizerbart'sche Verlagsbuchhandlung, Stuttgart*.
9. W.M. Dressel and H. Kenworthy: *Thermal Behavior of Manganese Minerals in Controlled Atmospheres*, vol. 5761, US Dept. of the Interior. Bureau of Mines, 1961.
10. K.L. Berg and S.E. Olsen: *Metall. Mater. Trans. B*, 2000, vol. 31, pp. 477–90.
11. Y.B. Gao, H.G. Kim, and H.Y. Sohn: *Miner. Process. Extract. Metall.*, 2012, vol. 121, pp. 109–16.
12. M. Tangstad, S. Wasbø, and R. Tronstad: in *Conference proceedings, Infacon IX (Quebec)*, 2001, pp. 202–07.
13. K. Turkova, D. Slizovskiy, and M. Tangstad: *ISIJ Int.*, 2014, vol. 54, pp. 1204–08.
14. S. Lobo: *Reduction of Manganese Ores Using CO, H2, CO2 and H2O Blends*, 2015.
15. M. Tangstad: *Summary of Prereduction Experiments in the Disvadri Furnaces with Industrial Materials in Gasferrosil v.2*, NTNU, 2017.
16. G. Pochart, L. Joncourt, N. Touchard, and C. Perdon: *World*, 2007, vol. 800, p. 1200.
17. T.J.W. De Bruijn, T.H. Soerawidjaja, W.A. De Jongt, and P.J. Van Den Berg: *Chem. Eng. Sci.*, 1980, vol. 35, pp. 1591–99.
18. D.E. Newbury and N.W. Ritchie: *Scanning*, 2013, vol. 35, pp. 141–68.
19. D.E. Newbury and N.W. Ritchie: in *Scanning Microscopies 2011: Advanced Microscopy Technologies for Defense, Homeland Security, Forensic, Life, Environmental, and Industrial Sciences*, vol. 8036, International Society for Optics and Photonics, 2011, p. 803602.
20. P. Kowitwarangkul, A. Babich, and D. Senk: *Steel Res. Int.*, 2014, vol. 85, pp. 1501–09.
21. C. Naganna: in *Proceedings of the Indian Academy of Sciences-Section A*, vol. 58, Springer, 1963, pp. 16–28.
22. O. Biørnstad: MSc thesis, NTNU, 2020.